JOURNAL OF MATERIALS SCIENCE 27 (1992) 3565 3569

Viscous flow behaviour of Ni_xZr_{100-x} metallic glasses from $Ni_{30}Zr_{70}$ to $Ni_{64}Zr_{36}$

K. RUSSEW, F. SOMMER, P. DUHAJ*, I. BAKONYI
Max-Planck-Institut für Metallforschung, Institut für Werkstoffwissenschaft, Seestraße 92, D-7000 Stuttgart 1, Germany
**Institute of Physics of EPRC, Slovak Akademy of Sciences, Dubravska Cesta 9, 842 28 Bratislava, Czechoslovakia*

The compositional dependence of viscous flow in the Ni_xZr_{100-x} amorphous system was investigated under non-isothermal conditions at a heating rate of 10 K min^{-1} in the compositional range from $x = 30$ to $x = 64$ at% with the aid of a Hereaus TMA 500 dilatometer. The crystallization behaviour of the same glassy alloys under the same non-isothermal conditions was studied with a Perkin–Elmer DSC 7 differential scanning calorimeter. The characteristic crystallization and viscous flow parameters (the onset temperature, T_x, of crystallization; the temperature, T_m, of maximum heat evolution of the first crystallization step; the enthalpy, ΔH_x, of crystallization; the activation energy, Q_x, of crystallization; the glass transition temperature, T_g; the viscosity values η (T_g) and η_{min}; and the activation energy for viscous flow Q_η ($T > T_g$), were shown to be dependent on composition. This dependence was examined on the basis of the equilibrium phase diagram of the Ni–Zr-system, and it is shown that glassy alloys possessing eutectic compositions manifest the greatest thermal stability because of the long-range atomic diffusion needed for crystallization to occur. Glassy alloys with nearly peritectoid compositions show low thermal stability, as no long-range diffusion is needed for the formation of the stable crystallization end-products $NiZr_2$ and NiZr. In all cases, the crystallization process is governed by viscosity flow of these glassy alloys.

1. Introduction

Metallic glasses fall conventionally into two categories, metal–metalloid systems such as Fe–B, Co–P, Pd–Si, etc., and purely metallic systems such as Ni–Zr, Fe–Zr, Cu–Ti, Cu–Zr etc. Of these two types of amorphous alloy, the former have received more attention because of their potential technical applications. However, the latter type is more attractive for study of the fundamental properties of glassy metals, as the purely metallic amorphous alloys can usually be prepared over a wide range of compositions, making it possible to study systematic changes of properties as a function of composition within one alloy system. In the case of the Ni–Zr amorphous system, such systematic studies have been carried out with respect to glass formation, stability and crystallization [1–3], hydrogen absorption [4], superconducting transition temperature and magnetic susceptibility [5], short-range order of mechanically alloyed amorphous Ni–Zr [6], diffusion [7–9], and extended X-ray absorption fine-structure (EXAFS) measurements, in order to understand the local structure against composition [10], comparisons between the thermal properties of Ni–Zr amorphous alloys obtained by mechanical alloying and melt spinning [11], etc. No systematic studies of the viscous flow behaviour as a function of composition for Ni–Zr metallic glasses have been carried out to our knowledge, the only exception being the study of viscous flow of $Ni_{30}Zr_{70}$ metallic glass [12].

Here we describe a study of the viscous flow behaviour of Ni_xZr_{100-x} ($x = 30, 40, 50, 64$ at %) melt-spun amorphous alloys with the aid of nonisothermal dilatometry.

2. Experimental procedure

The glassy alloys used in this study were melt-spun $Ni_{30}Zr_{70}$, $Ni_{40}Zr_{60}$, $Ni_{50}Zr_{50}$ and $Ni_{64}Zr_{36}$ ribbons with the dimensions (with x thickness) 1×0.0285, 1.0×0.028, 2×0.038 and 1.5×0.028 mm, respectively. Viscosity measurements were carried out using a Heraeus TMA 500 silica glass dilatometer with an assembly for creep measurements, shown schematically in Fig. 1. The upper stationary grip is connected, via a specially designed silica glass rod with a hook at the end, to the core of a linear variable differential transformer (LVDT). The LVDT is used to measure the displacement due to the thermal elongation and/or viscous flow of the specimen. The core is in turn connected to the loading platform on which weights up to 0.1 kg can be applied. The dilatometer furnace possesses a 10-cm hot zone over which the temperature profile is constant with $\pm$ 1 K.

0022–2461

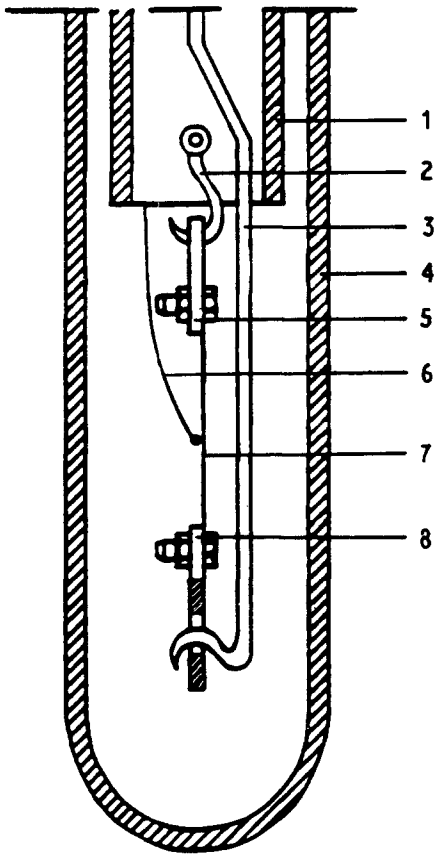

Figure 1 Schematic diagram of the silica glass assembly for creep measurements of the Heraeus TMA 500 dilatometer. 1, supporting silica glass tube; 2, silica glass hook; 3, silica glass rod with hook at end for applying load and connecting moving grip to LVDT-core; 4, protecting silica glass tube; 5, stationary grip of the Invar alloy; 6, thermocouple; 7, specimen; 8, moving grip of Invar alloy. Measurements are carried out in inert atmosphere with Ar as purging gas.

In order to study viscous flow in the Ni_xZr_{100-x} amorphous system, 20-mm-long pieces of ribbon of each alloy composition were used. For each creep test the average result for three samples was used. The elongation–temperature (time) curves of these specimens under applied loads of 0.05 and 0.1 kg, respectively, under a constant heating rate of 10 K min^{-1}, were monitored up to temperatures higher than the temperature of fully completed crystallization. In a previous paper [13] we showed that by subtracting the overall strain, ε_1, caused by an applied stress, σ_1, under continuous heating conditions from the overall strain, ε_2, caused by an applied stress, σ_2, $\sigma_2 > \sigma_1$ under the same continuous heating conditions the contributions of thermal expansion, relaxation and elastic and anelastic strains to the overall strain could be eliminated or neglected, and the difference $\Delta\varepsilon_{1,2}$ considered as a pure viscous flow contribution to the overall strain. This contribution is caused by an effective stress $\Delta\sigma_{1,2} = \sigma_2 - \sigma_1$. This is why, under the same constant heating rate conditions, the overall strains $\varepsilon_{0.1}$ and $\varepsilon_{0.05}$ caused by loads of 0.1 and 0.05 kg, respectively, were experimentally determined from the elongation–temperature (time) curves, and also why the difference $\Delta\varepsilon_{0.05}$ as a function of temperature (time) was used in order to calculate the strain rate $\Delta\dot{\varepsilon}_{0.05}$ and viscosity of the ribbons tested. For this purpose, the strain–temperature (time) curves were fitted piecewise by second to fifth degree polynomials, and the values of the strain rate were obtained from the derivatives of the fitted functions. The apparent viscosity, η, was calculated at different temperatures using Newton's equation

$$\eta = \sigma_{0.05}/3\Delta\dot{\varepsilon}_{0.05} \quad (1)$$

Due to the different dimensions of the ribbons, the normal stresses $\Delta\sigma_{0.05}$ causing the viscous flow were also different, being equal to 89.4, 89.4, 59.5 and 119 MPa for $Ni_{30}Zr_{70}$, $Ni_{40}Zr_{60}$, $Ni_{50}Zr_{50}$ and $Ni_{64}Zr_{36}$, respectively. The apparent activation energy for viscous flow Q_η was calculated from the slope of an Arrhenius plot of log viscosity against reciprocal temperature.

A Perkin–Elmer DSC 7 differential scanning calorimeter was used to study the crystallization behaviour of Ni–Zr amorphous alloys at heating rates of 5, 10 and 30 K min^{-1}, respectively. In order to demonstrate the extent to which the crystallization process in the alloys studied is governed by viscous flow, the activation energies for crystallization Q_x and viscous flow Q_η, respectively, were compared. For this purpose the temperatures, T_m, at which maximum heat evolution due to the first crystallization step at the different scanning rates is observed were determined, and the activation energy for crystallization, Q_x, was calculated using the method proposed by Kissinger [14].

3. Results and discussion

The temperature (time) dependence of viscous strains $\Delta\varepsilon_{0.05}$ obtained from the elongation–temperature (time) curves of the Ni_xZr_{100-x} samples, under applied loads of 0.1 and 0.5 kg, are shown in Fig. 2. The amount of strain depends on both the applied stress and the alloy composition, but the compositional dependence is strongest. For the case of $Ni_{40}Zr_{60}$ and $Ni_{64}Zr_{36}$ amorphous alloys, the strains are up to an order of magnitude higher than those observed for $Ni_{30}Zr_{70}$ and $Ni_{50}Zr_{50}$ amorphous alloys. This can be explained with the aid of the Ni–Zr equilibrium phase diagram given by Altounian *et al.* [2], and with a knowledge of the nature and number of crystallization products of glassy Ni–Zr. The $Ni_{40}Zr_{40}$ and $Ni_{64}Zr_{36}$ amorphous alloys possess nearly eutectic composi-

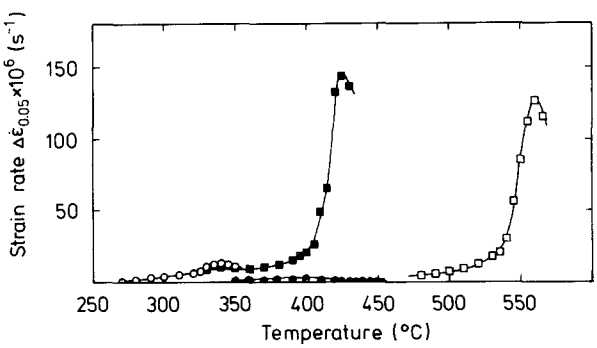

Figure 2 Temperature dependence of the viscous strain contributions $\Delta\varepsilon_{0.05}$ for the Ni_xZr_{100-x} glassy alloys: ○, $Ni_{30}Zr_{70}$, $\Delta\sigma_{0.05}$ = 89.4 MPa; ■, $Ni_{40}Zr_{60}$, $\Delta\sigma_{0.05}$ = 89.4 MPa; ●, $Ni_{50}Zr_{50}$, $\Delta\sigma_{0.05}$ = 59.5 MPa; □, $Ni_{64}Zr_{36}$, $\Delta\sigma_{0.05}$ = 119 MPa.

tions, which correlates with better glass-forming ability and thermal stability. Our DSC results, which are in good agreement with the results of Altounian *et al.* [2], show that $Ni_{40}Zr_{60}$ and $Ni_{64}Zr_{36}$ exhibit complex DSC exotherms with three and two crystallization stages, respectively. The final crystallization products according to [2] are $NiZr_2$ + NiZr and $Ni_{10}Zr_7$ + Ni_2Zr, respectively. The complex structures and the number of crystallization products of the above mentioned glassy alloys require long-range atomic rearrangements, which are possible only when sufficiently high temperatures are reached (high thermal stability). The higher the temperature, the lower the viscosity of the glassy structure. As a consequence of the low viscosity values reached before the onset of crystallization, high strain levels are also reached before the crystallization starts . In the case of $Ni_{30}Zr_{70}$ and $Ni_{50}Zr_{50}$ glassy alloys, however, whose compositions are very near to or practically coincide with the compositions of the peritectoid phases ($NiZr_2$ and NiZr [2], respectively) no long-range atomic diffusion of the large Zr atoms is needed for the formation of these crystalline compounds. As a result, crystallization becomes possible at lower temperatures (low thermal stability) and at higher viscosity values. The amount of strain reached before the onset of crystallization is consequently much smaller than that reached before the onset of crystallization of nearly eutectic $Ni_{40}Zr_{60}$ and $Ni_{64}Zr_{36}$ glassy alloys.

Fig. 3 shows the temperature dependence of the flow rates $\Delta\varepsilon_{0.05}$ for the Ni–Zr glassy alloys studied. All strain rate–temperature curves show an initial weak increase with temperature up to a specific temperature, which generally increases with increasing Ni content, after which a rapid increase in the strain rate is observed with an inflection point corresponding approximately to the onset temperature of crystallization. At temperatures which correspond approximately to the temperatures, T_m, of maximum heat evolution due to the first crystallization stage, the strain rates reach a maximum after which shrinkage due to crystallization prevails. The compositional dependence of strain rates is very well defined. The strain rate of $Ni_{40}Zr_{60}$ is almost 10^2 times higher than the strain rate of $Ni_{50}Zr_{50}$ glassy alloy. An explanation for this phenomenon is given above when considering the compositional dependence of strain (Fig. 2).

The temperature dependence of the apparent viscosity, η, of the glassy Ni–Zr alloys studied is shown in Fig. 4 in a plot of ln η against 1000 T^{-1}. A common feature of all viscosity temperature dependences is the existence of two linear parts with different slopes. The cross-over temperature is considered as the glass transition temperature T_g. At temperatures higher than the onset temperature of crystallization T_x, the values of η are influenced by the increasing volume fraction ξ of crystalline regions along with increasing temperature. As a result, viscosity values go through a minimum and then increase rapidly. For the calculation of the true viscosity in this case, the Einstein equation for the flow of mixtures should be used [15, 16]

$$\eta_{eff} = \eta(1 + 2.5\xi) \quad (2)$$

Here η_{eff} is the viscosity of a mixture consisting of a small volume fraction, ξ, of spherical particles suspended in a medium of viscosity η. No corrections of the apparent viscosity values with Equation 2 were made in this study, as the second linear parts of the viscosity–temperature dependences (with the exception of $Ni_{50}Zr_{50}$ glassy alloy) were considered as well defined enough to calculate the activation energy for viscous flow from their slopes at temperatures higher than T_g, e.g. in the temperature range where the glassy alloys studied reach the quasi-equilibrium state of undercooled liquids [13].

The most characteristic parameters of crystallization and viscous flow processes in the Ni–Zr glassy alloys studied are the onset temperature of crystallization T_x; the temperature T_m at which maximum heat evolution due to the first crystallization stage is observed; the enthalpy ΔH_x of crystallization; the activation energy for crystallization Q_x; the glass-transition temperature T_g; the viscosity values η (T_g) at the glass transition temperature; the minimum viscosity values reached during the course of crystallization; and the activation energies Q_η ($T < T_g$) and Q_η ($T > T_g$) of viscous flow at temperatures lower and higher than

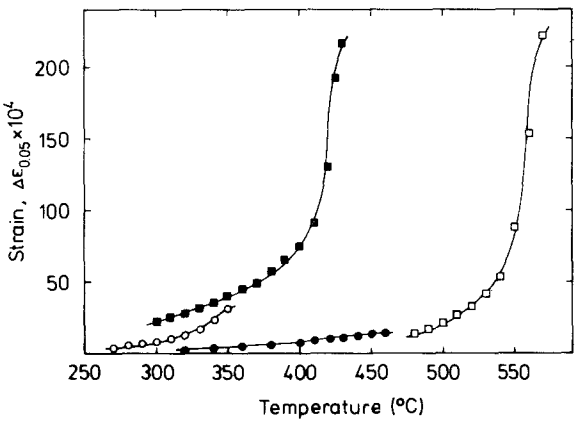

Figure 3 Temperature dependence of the flow rate $\Delta\varepsilon_{0.05}$ for the Ni_xZr_{100-x} glassy alloys: ○, $Ni_{30}Zr_{70}$; ◙, $Ni_{40}Zr_{60}$; ●, $Ni_{50}Zr_{50}$; □, $Ni_{64}Zr_{36}$.

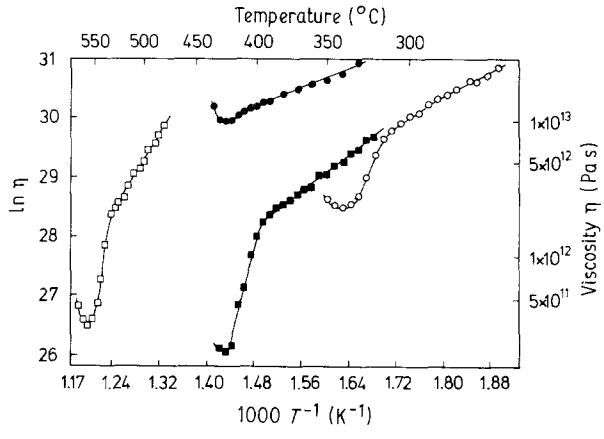

Figure 4 Temperature dependence of the viscosity η in coordinates ln(η) against (1000 T^{-1}) for the Ni_xZr_{100-x} glassy alloys: ○, $Ni_{30}Zr_{70}$; ■, $Ni_{40}Zr_{60}$; ●, $Ni_{50}Zr_{50}$; □, $Ni_{64}Zr_{36}$.

TABLE I Compositional dependence of the main characteristic parameters of crystallization and viscous flow in the glassy Ni_xZr_{100-x} system

Parameter	x (at %)			
	30	40	50	64
Number of DSC-peaks	1	3	1	2
T_x (°C)	339	411	387	572
T_m of 1st peak (°C)	344	421	401	578
ΔH_x (kJ mol^{-1})	− 4.45	− 3.47	− 6.75	− 6.48
Q_x in (kJ mol^{-1})	202	371	170	478
T_g (°C)	315	395	410	535
η (T_g) (Pa s)	7.3×10^{12}	1.8×10^{12}	1.2×10^{13}	2.1×10^{12}
η_{min} (Pa s)	2.3×10^{12}	2.1×10^{11}	1×10^{13}	3×10^{11}
Q_η ($T < T_g$) (kJ mol^{-1})	54	62	32	141
Q_η ($T > T_g$) (kJ mol^{-1})	190	398	66	508

the glass transition temperature, respectively. These characteristic parameters are given in Table I as functions of composition. Our calorimetric results are in fairly good agreement with the results of Altounian *et al.* [2]. The activation energy for crystallization Q_x (202 kJ mol^{-1}) and the activation energy for viscous flow Q_η (190 kJ mol^{-1}) for the case of the $Ni_{30}Zr_{70}$ glassy alloy as obtained by us are in very good agreement with the activation energy for crystallization, as determined by Kolb-Telieps and Shu-Song [17] ($Q_x = 180 \div 254$ kJ mol^{-1}) and by Scott *et al.* [18] ($Q_x = 200$ kJ mol^{-1}) for the same alloy composition. This is not the case for the activation energies Q_x ($Q_x \simeq 342/394$ kJ mol^{-1}) obtained by Fu-Qian [12], who has studied the viscous flow and DSC measurements of the $Ni_{30}Zr_{70}$ glassy alloy. There are also great discrepancies in the onset temperature of crystallization T_x and in the minimum viscosity values η_{min}, which in our case are two orders of magnitude higher than the values reported in [11]. The reason for these discrepancies remains unclear.

From a comparison of the activation energy for crystallization Q_x with the activation energy for viscous flow Q_η, we can conclude that, with the exception of the $Ni_{50}Zr_{50}$ glassy alloy, these activation energies are practically equal, i.e. the rate-controlling process of crystallization is viscous flow. A possible explanation for the discrepancy between Q_x and Q_η in the case of the $Ni_{50}Zr_{50}$ glassy alloy could be that the glass transition temperature of this alloy (410 °C) is much higher than the onset temperature of crystallization T_x (378 °C). As a result, glass transition is observed only after more than 50% of the amorphous matrix is crystallized, and Equation 2 is no longer valid for making corrections to the apparent viscosity values [14, 15]. Taking this into account, the value of 66 kJ mol^{-1} obtained for the activation energy for viscous flow at temperatures higher than T_g could not be considered as realistic. The fact that the crystallization of the $Ni_{50}Zr_{50}$ glassy alloy takes place in a frozen amorphous structural state, and not after the structural state of undercooled liquid is reached, supports the assumption that no long-range atomic rearrangements are needed in the process of crystallization of this glassy alloy.

4. Conclusions

1. The viscous flow behaviour of Ni_x–Zr_{100-x} glassy alloys over a range of compositions from 30 to 64 at % Ni shows very well defined compositional dependence, which could be explained with the aid of the equilibrium-phase diagram of this alloy system.

2. The thermal stability of the glassy phase is greatest for the range of eutectic compositions ($x = 40$ and $x = 64$ at %, respectively). This is due to the long-range atomic diffusion needed for the crystallization of at least two crystallization products.

3. Glassy Ni_xZr_{100-x} alloys with compositions which correspond to the peritectoid phases, $NiZr_2$ and NiZr ($x = 30$ and 50 at %, respectively), show low thermal stability. This is due to the fact that no long-range diffusion of the large Zr atoms is needed for the formation of the stable crystallization end products, $NiZr_2$ and NiZr.

4. In all cases, the crystallization process is governed by viscous flow in the glassy alloys.

5. Viscous flow measurements can be used as a sensitive tool for study of property changes against composition in amorphous metallic alloys.

Acknowledgements

K. R. is grateful to the Alexander von Humboldt Foundation, Germany, and to the Max-Planck-Gesellschaft, Germany, for a research fellowship and financial support during this study. A. Lovas (Central Research Institute for Physics, Budapest) is acknowledged for preparing the $Ni_{50}Zr_{50}$ glassy alloy.

References

1. Y. D. DONG, G. GREGAN and M. G. SCOTT, *J. Non-Cryst. Solids* **43** (1981) 403.
2. Z. ALTOUNIAN, TU GUO-HUA and J. O. STROM-OLSEN, *J. Appl. Phys.* **54** (1983) 3111.
3. K. H. J. BUSCHOW, *J. Phys. F: Metalphys.* **14** (1984) 593.
4. T. ARAKI, T. ABE and K. TANAKA, *Mater. Trans. JIM* **30** (1989) 748.
5. Z. ALTOUNIAN and J. O. STROM-OLSEN, *Phys. Rev. B* **27** (1983) 4149.
6. A. BURBLIES and F. PETZOLDT, *J. Non-Cryst. Solids* **107** (1989) 233.

7. S. K. SHARMA and P. MUKHOPADHYAY, *Acta Metall. Mater.* **38** (1990) 129.
8. H. HAHN and R. S. AVERBACK, *Phys. Rev. B* **37** (1988) 6533.
9. K. HOSHINO, R. S. AVERBACK, H. HAHN and S. J. ROTHMAN, *J. Mater. Res.* **3** (1988) 55.
10. H. MAEDA, T. FUKUNAGA, K. SUZUKI, K. OSAMURA, M. HIDA, H. TERAUCHI and NOGAO KAMIJO, *Jpn. J. Appl. Phys.* **27** (1988) L 938.
11. R. BRÜNING, Z. ALTOUNIAN and J. O. STROM-OLSEN, *Mater. Sci. Engng* **97** (1988) 317.
12. Z. FU-QIAN, *ibid.* **97** (1988) 487.
13. K. RUSSEW and L. STOJANOVA, *ibid.* **A123** (1990) 59.
14. H. E. KISSINGER, *Anal. Chem.* **29** (1957) 1702.
15. J. P. PATTERSON and D. R. H. JONES, *Acta Metall.* **28** (1980) 675.
16. S. S. TSAO and F. SPAEPEN, *ibid.* **33** (1985) 881.
17. A. KOLB-TELIEPS and TAH SHU-SONG, *J. Non-Cryst. Solids* **107** (1988) 122.
18. M. G. SCOTT, G. GREGAN and Y. D. DONG, in Proceedings of the 4th Conference on Rapidly Quenched Metals, Sendai, 1981, edited by T. Masumoto and K. Suzuki (Institute of Metals, Sendai, 1982) p. 671.

Received 24 February
and accepted 1 September 1991